

Determining the WIMP mass using direct detection experiments

Anne M. Green[†]

[†] School of Physics and Astronomy, University of Nottingham, University Park, Nottingham, NG7 2RD, UK

E-mail: anne.green@nottingham.ac.uk

,

Abstract.

We study the accuracy with which the WIMP mass could be determined by a superCDMS-like direct detection experiment, given optimistic assumptions about the detector set-up and WIMP properties. We consider WIMPs with an interaction cross-section of $\sigma_p = 10^{-7}$ pb (just below current exclusion limits) and assume, initially, that the local WIMP velocity distribution and density are known and that the experiment has zero background. For light WIMPs (mass significantly less than that of the target nuclei) small variations in the WIMP mass lead to significant changes in the energy spectrum. Conversely for heavy WIMPs the energy spectrum depends only weakly on the WIMP mass. Consequently it will be far easier to measure the WIMP mass if it is light than if it is heavy. With exposures of $\mathcal{E} = 3 \times 10^3, 3 \times 10^4$ and 3×10^5 kg day (corresponding, roughly, to the three proposed phases of SuperCDMS) it will be possible, given the optimistic assumptions mentioned above, to measure the mass of a light WIMP with an accuracy of roughly 25%, 15% and 2.5% respectively. These numbers increase with increasing WIMP mass, and for heavy WIMPs, $m_\chi > \mathcal{O}(500 \text{ GeV})$, even with a large exposure it will only be possible to place a lower limit on the mass. Finally we discuss the validity of the various assumptions made, in particular regarding the smoothness of the small scale WIMP distribution, and the consequences if these assumptions are not valid.

Keywords: dark matter, dark matter detectors

1. Introduction

Diverse cosmological observations indicate that the majority of the matter in the Universe is dark and non-baryonic (e.g. Ref. [1]). Weakly Interacting Massive Particles (WIMPs) are one of the leading cold dark matter candidates, and supersymmetry provides a concrete, well-motivated, WIMP candidate in the form of the lightest neutralino (e.g. Ref. [2, 3]). The direct detection of WIMPs in the lab [4] would not only directly confirm the existence of dark matter but would also probe the parameters of supersymmetry. Constraints on or measurements of the WIMP mass and interaction cross-section would be complementary to the information derived from collider experiments [5, 6]. It is therefore pertinent to examine the accuracy with which WIMP direct detection experiments will be able to measure the WIMP mass, if they detect WIMPs.

Direct detection experiments could potentially measure the WIMP mass via the mass dependence of either the energy spectrum [7] or the ‘crossing energy’ at which the phase of the annual modulation signal [8], due to the motion of the Earth, changes sign [9, 10, 11]. The size of the annual modulation signal is small (of order a few percent), however, and given the current exclusion limits from CDMS [12, 13] it is unlikely that even planned tonne scale experiments, such as SuperCDMS [14, 15], Xenon [16] and EURECA [17], will be able to accurately measure the energy dependence of the annual modulation phase [10, 18] ‡. The mass dependence of the differential event rate [7] (see also [20]) therefore appears to offer the best prospect, in the short to medium term at least, for probing the WIMP mass using direct detection experiments.

In this paper we examine the accuracy with which a future SuperCDMS [14, 15] like direct detection experiment will be able to measure the WIMP mass, given a positive detection. We consider the effect of varying the underlying WIMP mass and detector exposure, and also examine the uncertainties which arise from our lack of knowledge of the underlying WIMP distribution. In Sec. 2 we outline the calculation of the different event rate and its dependence on the WIMP mass. We describe our Monte Carlo simulations and results in Sec. 3, discuss the validity of the assumptions made in Sec. 4 and conclude with discussion in Sec. 5.

2. Differential event rate

2.1. Basic calculation

The direct detection differential event rate, or energy spectrum, depends on the WIMP mass, its interaction with the detector nuclei and the velocity distribution of the incoming WIMPs. Assuming purely spin-independent coupling, the event rate per unit

‡ The DAMA collaboration have, with a NaI detector and an exposure of $\sim 1.1 \times 10^5$ kg day, observed an annual modulation, which they interpret as a WIMP signal [19], however it appears to be possible to reconcile this with the CDMS exclusion limit only by invoking non-standard WIMP properties.

energy, is given by (see e.g. [2, 7]):

$$\frac{dR}{dE}(E) = \frac{\sigma_p \rho_\chi}{2\mu_{p\chi}^2 m_\chi} A^2 F^2(E) \mathcal{F}(E), \quad (1)$$

where ρ_χ is the local WIMP density, σ_p the WIMP scattering cross section on the proton, $\mu_{p\chi} = (m_p m_\chi) / (m_p + m_\chi)$ the WIMP-proton reduced mass, A and $F(E)$ the mass number and form factor of the target nuclei respectively and E is the recoil energy of the detector nucleus. The dependence on the WIMP velocity distribution is encoded in $\mathcal{F}(E)$, which is defined as

$$\mathcal{F}(E) = \langle \int_{v_{\min}}^{\infty} \frac{f_v(t)}{v} dv \rangle, \quad (2)$$

where $f_v(t)$ is the (time dependent) WIMP speed distribution in the rest frame of the detector, normalized to unity and $\langle \dots \rangle$ denotes time averaging. The lower limit of the integral, v_{\min} , is the minimum WIMP speed that can cause a recoil of energy E :

$$v_{\min} = \left(\frac{Em_A}{2\mu_{A\chi}^2} \right)^{1/2}, \quad (3)$$

where m_A is the atomic mass of the detector nuclei and $\mu_{A\chi}$ the WIMP-nucleon reduced mass. We use the Helm form factor [21] with parameter values as advocated by Lewin and Smith [7]. For most calculations we use the ‘standard halo model’, an isotropic isothermal sphere, for which the local WIMP speed distribution, in the Galactic rest frame, is Maxwellian (c.f. Ref. [8])

$$f(v) = N \left[\exp(-v^2/v_c^2) - \exp(-v_{\text{esc}}^2/v_c^2) \right] \quad v < v_{\text{esc}}, \quad (4)$$

$$f(v) = 0 \quad v > v_{\text{esc}}, \quad (5)$$

where N is a normalization factor, $v_c = 220 \text{ km s}^{-1}$ [22] and $v_{\text{esc}} = 540 \text{ km s}^{-1}$ [23] are the local circular and escape speeds respectively and we use the usual fiducial value for the local WIMP density, $\rho_\chi = 0.3 \text{ GeV cm}^{-3}$. We use the expressions for the time dependence of the Earth’s velocity with respect to the Galactic rest frame from Ref. [7], to transform the speed distribution into the lab frame.

2.2. Dependence on the WIMP mass

The WIMP mass dependence of the differential event rate can most easily be seen, following Lewin and Smith [7], by first neglecting the Earth’s speed and the Galactic escape speed. In this case eq. (1) can be written as

$$\frac{dR}{dE}(E) = \left(\frac{dR}{dE} \right)_0 \exp \left(-\frac{E}{E_R} \right) F^2(E), \quad (6)$$

where $(dR/dE)_0$, the event rate in the $E \rightarrow 0 \text{ keV}$ limit, and E_R , the characteristic energy scale, are given by

$$\left(\frac{dR}{dE} \right)_0 = \frac{\sigma_p \rho_\chi}{\sqrt{\pi} \mu_{p\chi}^2 m_\chi v_c} A^2, \quad (7)$$

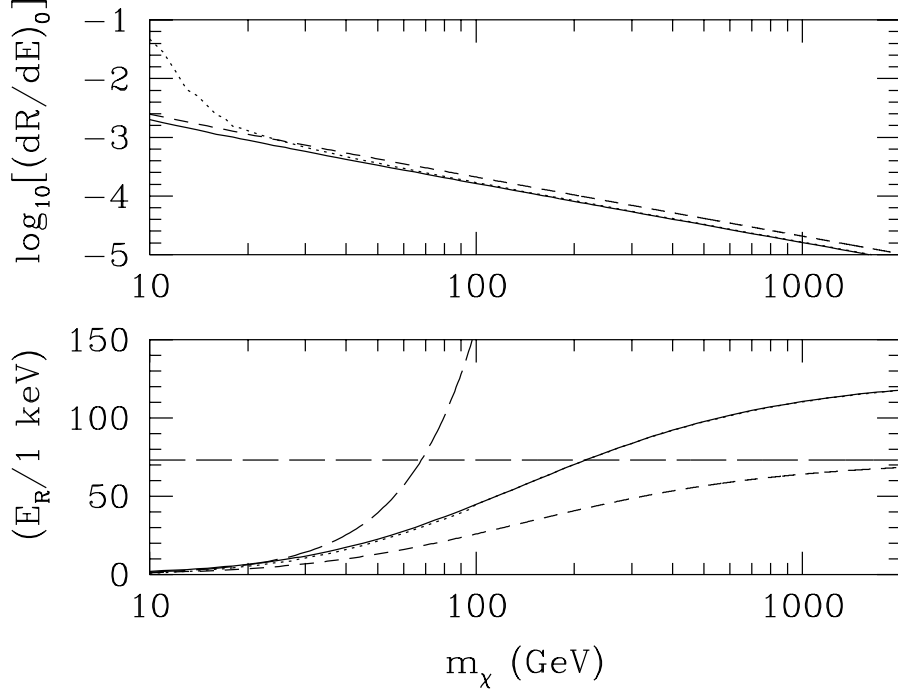


Figure 1. The differential event rate in the $E \rightarrow 0$ keV limit, $(dR/dE)_0$, (top panel) and the characteristic energy scale, E_R , (bottom panel) as a function of the WIMP mass, m_χ . The solid (dotted) lines are the fits to the full calculation including the Earth's velocity and the Galactic escape speed for threshold energy $E_{th} = 0$ (10) keV. The short dashed lines are eqs. (7) and (8) which neglect the Earth's velocity and the Galactic escape speed. In the bottom panel the long dashed lines are the asymptotic mass dependences of E_R in the $m_\chi \ll m_A$ and $\gg m_A$ limits ($E_R \propto m_\chi^2$ and $\propto \text{const}$ respectively).

and

$$E_R = \frac{2\mu_{A\chi}^2 v_c^2}{m_A}, \quad (8)$$

respectively. When the Earth's velocity and the Galactic escape velocity are taken into account eq. (1) is still a reasonable approximation to the event rate, provided that fitting constants of order unity, c_0 and c_{E_R} , are incorporated into the expressions for $(\frac{dR}{dE})_0$ and E_R [7]. We find, using least squares fitting to the full numerically calculated time averaged differential event for a Ge detector with energy threshold $E_{th} = 0$ keV, $c_0 \approx 0.78$ and $c_{E_R} \approx 1.72$, with a weak dependence (in the 3rd significant figure) on the WIMP mass.

The mass dependence of $(dR/dE)_0$ and E_R are shown in fig. 1. As expected from eq. (7), $(dR/dE)_0 \propto m_\chi^{-1}$. Similarly as expected from eq. (8), for $m_\chi < \mathcal{O}(30 \text{ GeV})$, $E_R \propto m_\chi^2$. This mass dependence weakens with increasing WIMP mass, and E_R tends to its constant large mass asymptote for $m_\chi \sim \mathcal{O}(1 \text{ TeV})$. We will see below that this has important consequences for the determination of the WIMP mass from direct detection experiments. If, anticipating section III, we only fit to the event rate above

an energy threshold $E_{\text{th}} = 10 \text{ keV}$ we find that for WIMP masses below $\sim 100 \text{ GeV}$ the fitting constants depend on the WIMP mass (this is visible in fig. 1 as the deviation of the dotted lines from the solid lines for small WIMP masses). This illustrates that while eq. 6 is a useful approximation for demonstrating the mass dependence of the energy spectrum, for concrete applications the time average of the local WIMP velocity distribution should be calculated explicitly.

3. Monte Carlo simulations

We use Monte Carlo simulations to examine, for a range of detector exposures and input WIMP masses, how well the WIMP mass could be determined from the energies of observed WIMP nuclear recoil events.

3.1. Detector properties

Our simulated detector is based on the proposed SuperCDMS experiment [14, 15], being composed of Ge with a nuclear recoil energy threshold $E_{\text{th}} = 10 \text{ keV}$. We assume that the background event rate is zero, which is the experimental goal [14], and that the energy resolution is perfect. For simplicity we assume that the nuclear recoil detection efficiency is independent of energy. The energy dependence of the efficiency of the current CDMS experiment is relatively small (it increases from ~ 0.46 at $E = 20 \text{ keV}$, the energy above which data from all detectors is analyzed, to ~ 0.51 at 100 keV [13]). For further discussion of these assumptions see Sec. 4.

The proposed SuperCDMS detector consists of 3 phases, with detector masses of $\sim 25 \text{ kg}$, 150 kg and 1 ton . We consider efficiency weighted exposures $\S \mathcal{E} = 3 \times 10^2, 3 \times 10^3, 3 \times 10^4$ and $3 \times 10^5 \text{ kg day}$. The later three exposures correspond, roughly, to a detector with mass equal to that of the 3 proposed phases of SuperCDMS taking data for a year \parallel with a $\sim 50\%$ detection efficiency.

3.2. WIMP properties

We assume a fixed WIMP-nucleon cross-section of $\sigma_p = 10^{-7} \text{ pb}$, which is just below the current exclusion limit from the CDMS experiment [12]. Since the number of events expected in a given experimental set-up is directly proportional to the cross-section, there is a straight-forward scaling to other cross-sections i.e. an exposure $\mathcal{E} = 3 \times 10^4 \text{ kg day}$ for $\sigma_p = 10^{-7} \text{ pb}$ is equivalent to an exposure of $\mathcal{E} = 3 \times 10^5 \text{ kg day}$ for $\sigma_p = 10^{-8} \text{ pb}$. We consider input WIMP masses of $m_\chi = 25, 50, 100, 250$ and 500 GeV , with a Maxwellian speed distribution with circular speed $v_c = 220 \text{ km s}^{-1}$. For $m_\chi = 100 \text{ GeV}$ we also consider circular speeds in the range $v_c = 180$ to 260 km s^{-1} [22] and variations in the form of the speed distribution.

\S For brevity we subsequently refer to this as simply the exposure.

\parallel Accumulating this much ‘live-time’ would of course take substantially longer than a year.

3.3. Statistical analysis

For each exposure and input WIMP mass we simulate 10^4 experiments. We first calculate the expected number of events, $\lambda_{\text{in}} = \mathcal{E} \int_{E_{th}}^{\infty} (dR/dE) dE$, from the input energy spectrum. The actual number of events for a given experiment, N_{expt} , is drawn from a Poisson distribution with mean λ_{in} and we Monte Carlo generate N_{expt} events from the input energy spectrum. We then find the best fit WIMP mass and cross-section for each experiment by maximizing the log of the extended likelihood function (which takes into account the fact that the number of events in a given experiment is not fixed), e.g. Ref. [24],:

$$L = \frac{\lambda^{N_{\text{expt}}} \exp(-\lambda)}{N_{\text{expt}}!} \prod_{i=1}^{N_{\text{expt}}} f(E_i) \quad (9)$$

where E_i ($i = 1, \dots, N_{\text{expt}}$) are the energies of the events ‘observed’ in that experiment, $f(E)$ is the, normalized, differential event rate and $f(E)$ and λ depend on m_{χ} and σ_p .

Finally we plot the distribution of the pairs of best fit masses and cross sections. Given real data from a single experiment a Bayesian analysis with priors on the WIMP parameters, possibly based on the results of other experiments, would be a reasonable approach. However, the question which we are trying to address (‘For a given underlying WIMP mass, how well can the mass be measured?’) is best answered by simply considering the distribution of best-fit masses and cross-sections. Since the approximations we make regarding the detector set-up and WIMP distribution and cross-section are optimistic, our results provide upper limits on the accuracy with which a real experiment would be able to measure the WIMP mass.

3.4. Results

In fig. 2 we plot the distribution of best fit WIMP masses and cross-sections for input WIMP parameters $m_{\chi} = 100 \text{ GeV}$ and $\sigma_p = 10^{-7} \text{ pb}$. In this case both the input energy spectrum and the maximum likelihood analysis of the simulated events are carried out assuming a Maxwellian speed distribution with $v_c = 220 \text{ km s}^{-1}$. For each experiment the extended likelihood is maximized for WIMP parameters which produce an expected number of events approximately equal to the actual number of events observed in that experiment: $\lambda(m_{\chi}, \sigma_p) \approx N_{\text{expt}}$. This means that, for fixed exposure, the best fit parameters are localized on parabolas corresponding to fixed N_{expt} . For a given experiment the position of the best-fit parameters on the parabola depends on the durations of the observed events. For $\mathcal{E} = 3 \times 10^2 \text{ kg day}$, $\lambda_{\text{in}} = 7.8$, which is sufficiently small that the stratification of best fit parameters is clearly visible and we hence plot the actual pairs of $m_{\chi} - \sigma_p$ values. For the larger exposures the mean number of events expected is proportionately larger, the stratification is no longer visible, the best fit values are better localized in the $m_{\chi} - \sigma_p$ plane and we instead plot contours containing 68% and 95% of the simulated experiments.

For the two smallest exposures there is a significant tail of experiments with large best fit masses. This is due to the weak mass dependence of the characteristic energy

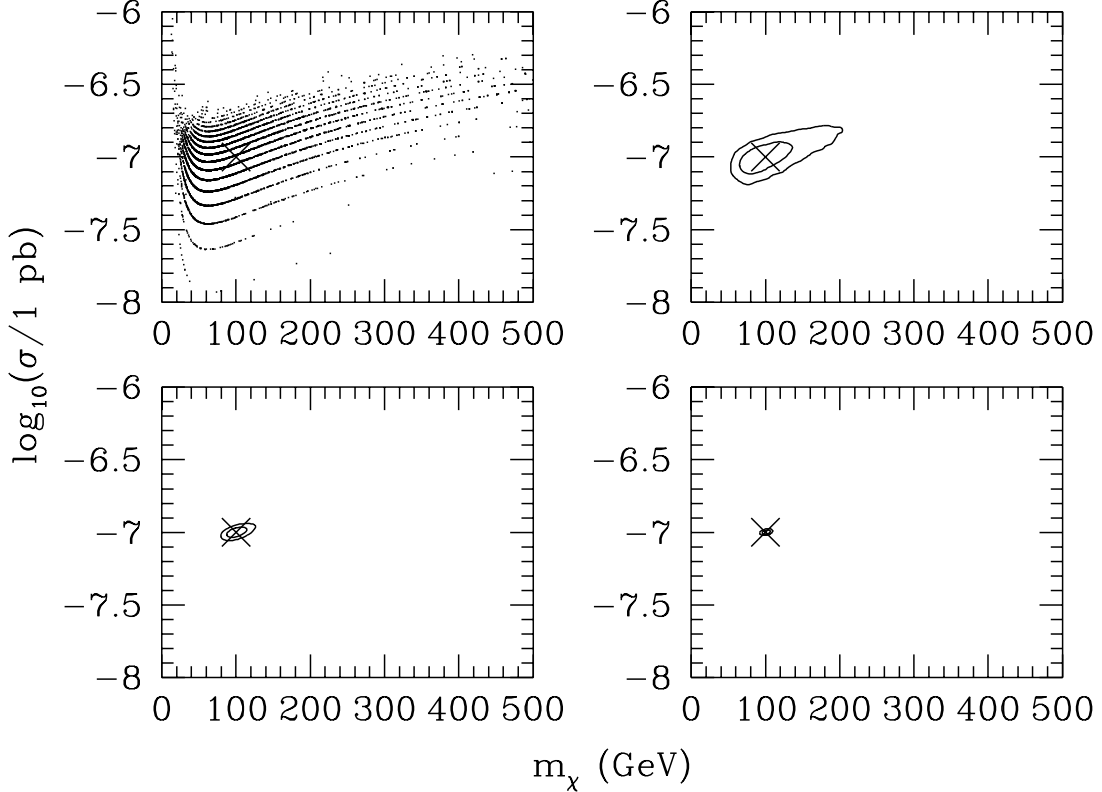


Figure 2. The distribution of the best fit WIMP masses, m_χ , and cross-sections, σ_p , for exposures of (top row, left to right and then bottom row left to right) $\mathcal{E} = 3 \times 10^2, 3 \times 10^3, 3 \times 10^4$ and 3×10^5 kg day. For $\mathcal{E} = 3 \times 10^2$ kg day we explicitly plot the results from all 10^4 Monte Carlo experiments. For the larger exposures we plot contours containing 68% and 95% of the simulated experiments. In each panel the large cross denotes the input parameters: $m_\chi = 100$ GeV, $\sigma_p = 10^{-7}$ pb.

E_R for $m_\chi > m_A$. Related to this, for these exposures the majority of experiments have best fit masses smaller than the input mass. The likelihood analysis is not biased, the expected value of the best fit mass is equal to the input mass, however there are a significant number of experiments with best fit masses substantially larger than the input mass. As the exposure is increased, λ_{in} becomes large and the fractional spread in the number of events observed in each experiment becomes small. This allows the interaction cross-section (which effectively acts as a normalization factor) to be accurately determined. The larger number of events also allows the energy dependence of the differential event rate, and hence the mass, to be determined more accurately.

With an exposure of $\mathcal{E} = 3 \times 10^2$ kg day and an underlying WIMP mass of $m_\chi = 100$ GeV it will be difficult to make quantitative statements about the WIMP mass, beyond excluding very large or very small masses. Similarly it will not be possible to measure the cross-section more accurately than to within an order of magnitude.

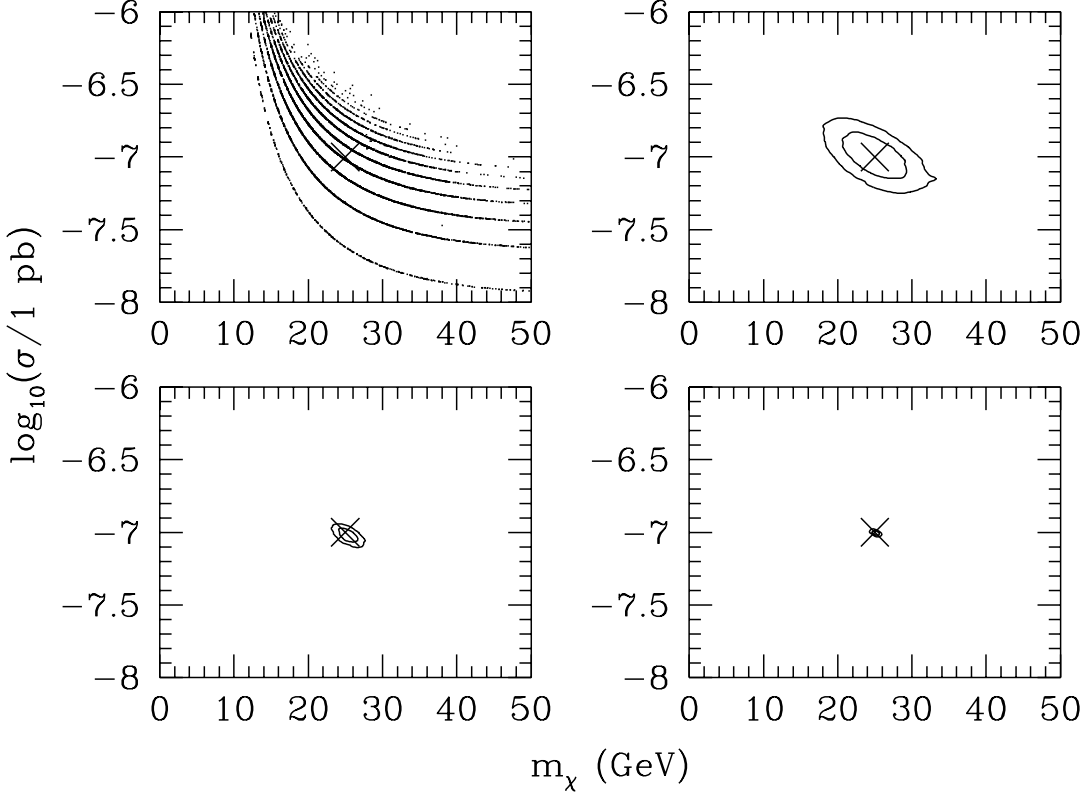


Figure 3. As fig. 2 for $m_\chi = 25$ GeV. For $\mathcal{E} = 3 \times 10^2$ kg day, $\lambda_{\text{in}} = 4.2$ and consequently $\sim 1\%$ experiments would not detect any events.

For $\mathcal{E} = 3 \times 10^3$ kg day the accuracy with which the mass can be determined improves, however there is still a significant tail of experiments finding best fit masses substantially larger than the underlying value. More quantitatively 95% of experiments will find best-fit masses in the range $60 \text{ GeV} < m_\chi < 200 \text{ GeV}$. Increasing the exposure by an order of magnitude, the distribution of best-fit masses becomes more symmetric about the input mass and the spread in the best fit masses is of order $\pm 30 \text{ GeV}$. With a further increase in the exposure to $\mathcal{E} = 3 \times 10^5$ kg day the mass could be measured to an accuracy of around 10 GeV (see the top panel of fig. 8 for a zoom in on the distribution in this case). The accuracy with which the cross-section can be measured increases with increasing exposure: $\Delta(\log \sigma_p) \sim \pm 0.2, 0.05$ and 0.02 for $\mathcal{E} = 3 \times 10^3, 3 \times 10^4$ and 3×10^5 kg day respectively. The shape of the distribution of best-fit parameters reflects the shape of parabolas of constant N_{expt} in the $m_\chi \sim 100$ GeV region, with a weak positive correlation between the best-fit values of m_χ and σ_p .

In figs. 3-6 we plot the results for input WIMP masses of $m_\chi = 25, 50, 250$ and 500 GeV respectively. For $m_\chi = 25, 250$ and 500 GeV the input mean number of events for $E = 3 \times 10^2$ kg day is small enough that a significant number of experiments will see no events (making it impossible to determine the WIMP mass in these experiments).

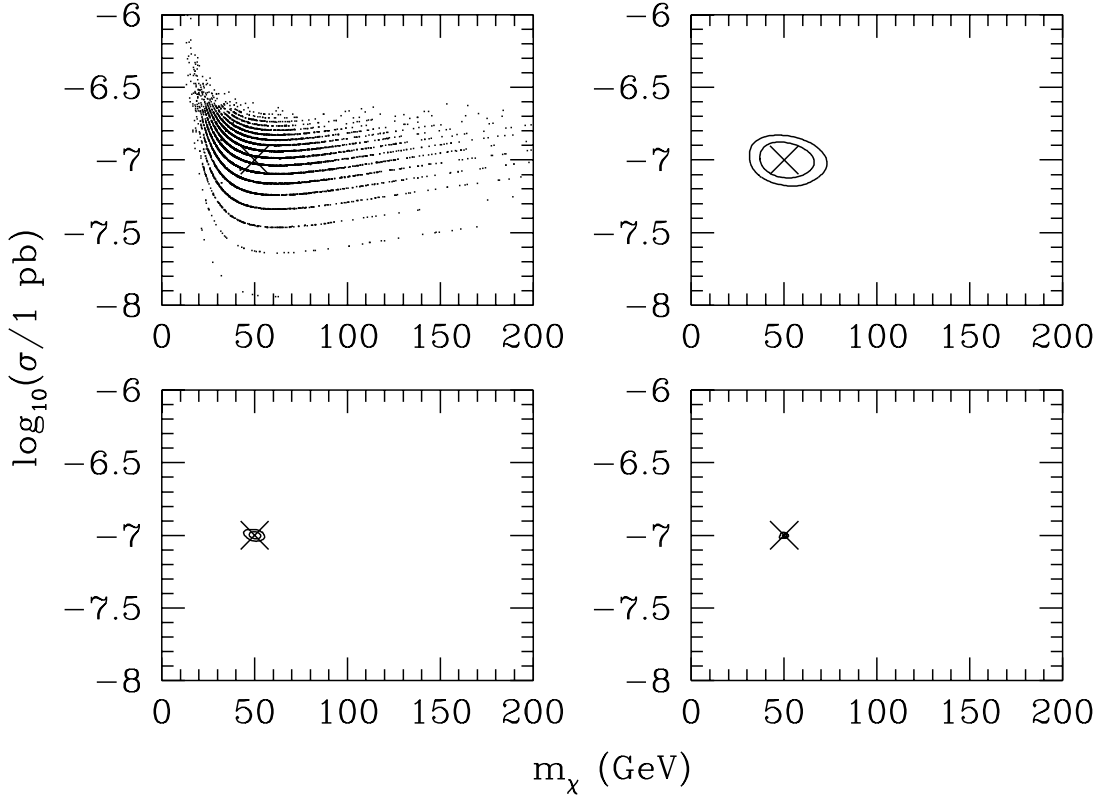


Figure 4. As fig. 2 for $m_\chi = 50$ GeV.

For light WIMPs, $m_\chi < m_A$, the characteristic energy, E_R , varies significantly with WIMP mass. This allows the mass to be determined with large exposures more accurately than for $m_\chi = 100$ GeV. For an underlying mass of $m_\chi = 25$ GeV and an exposure of $\mathcal{E} = 2 \times 10^3$ kg day, due to the small expected number of events, it will be difficult to place meaningful constraints (beyond an upper limit on the mass) on the WIMP parameters. With larger exposures it will be possible to measure the WIMP mass and cross-section with increasing accuracy; for $\mathcal{E} = 2 \times 10^3$, 2×10^4 and 2×10^5 kg day the distribution of best-fit WIMP masses is symmetric and 95% of experiments lie within $\pm 6, 4$ and 1 GeV of the input mass respectively. The accuracy with which σ_p can be measured improves roughly as for $m_\chi = 100$ GeV. For $m_\chi \sim 50$ GeV the fractional accuracy with which m_χ can be measured is similar; 95% of experiments lie within $\pm 12, 7, 2$ GeV of the input mass for $\mathcal{E} = 2 \times 10^3$, 2×10^4 and 2×10^5 kg day respectively. The parabolas of constant N_{expt} are, for $m_\chi = 50$ GeV, roughly parallel to the m_χ axis, improving slightly the accuracy with which σ_p can be measured.

For massive WIMPs, $m_\chi \gg m_A$, the weak dependence of E_R on the WIMP mass means that there is a large spread in the distribution of best fit masses even for large exposures. For an underlying WIMP mass of $m_\chi = 250$ GeV and an exposure of $\mathcal{E} = 2 \times 10^2$ kg day it will be difficult to place any meaningful constraints on the WIMP

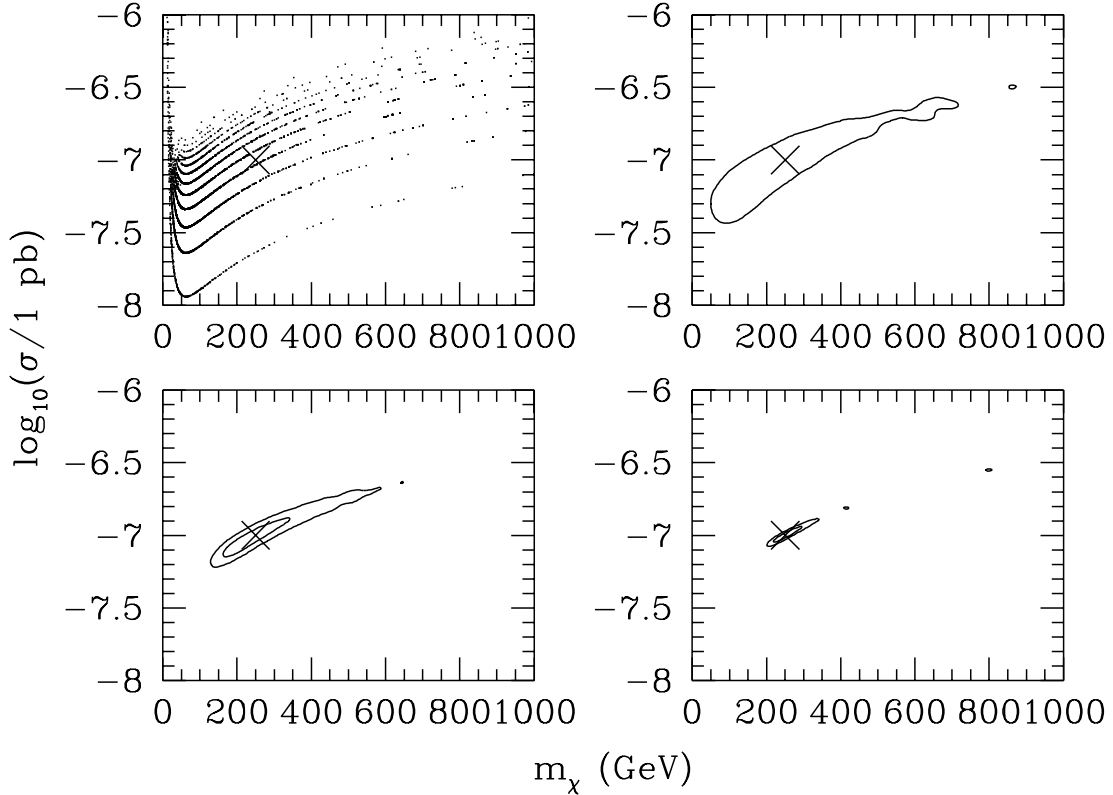


Figure 5. As fig. 2 for $m_\chi = 250$ GeV. For $\mathcal{E} = 3 \times 10^2$ kg day, $\lambda_{\text{in}} = 4.3$ and consequently $\sim 1\%$ of experiments would not detect any events. Even for $\mathcal{E} = 3 \times 10^5$ kg day there is a large tail of experiments with large m_χ values and hence it is not possible to plot a contour containing 95% of experiments. The disconnected ‘blobs’ at large m_χ are a consequence of the tail of experiments with large best-fit m_χ .

parameters. As the exposure is increased it will be possible to place a lower limit on the mass: for $\mathcal{E} = 2 \times 10^3$, 2×10^4 and 2×10^5 kg day, 95% of experiments have best fit mass greater than 50, 125 and 200 GeV respectively. However it will not be possible to place an upper limit tighter than $m_\chi < \mathcal{O}(1 \text{ TeV})$ on the WIMP mass with a reasonable degree of confidence. The shape of the parabolas of constant N_{exp} for $m_\chi \gg m_A$ mean that it will also be difficult to constrain σ_p . For $\mathcal{E} = 2 \times 10^4$ and 2×10^5 kg, 95% of experiments lie within $\Delta(\log \sigma_p) \approx \pm 0.4$ and ± 0.4 of the input value of σ_p (the asymmetric spread arises from the asymmetry in the distribution of best fit masses).

The situation is even worse for an underlying WIMP mass of $m_\chi = 500$ GeV. For $\mathcal{E} = 2 \times 10^3$ kg day it will not be possible to place any meaningful constraints on the WIMP parameters. For $\mathcal{E} = 2 \times 10^4$ and 2×10^5 kg day, 95% of experiments have best fit mass greater than 125 and 350 GeV respectively, however it will not be possible to place an upper limit on the WIMP mass at more than 68% confidence. Similarly it will only be possible to place a lower limit on σ_p .

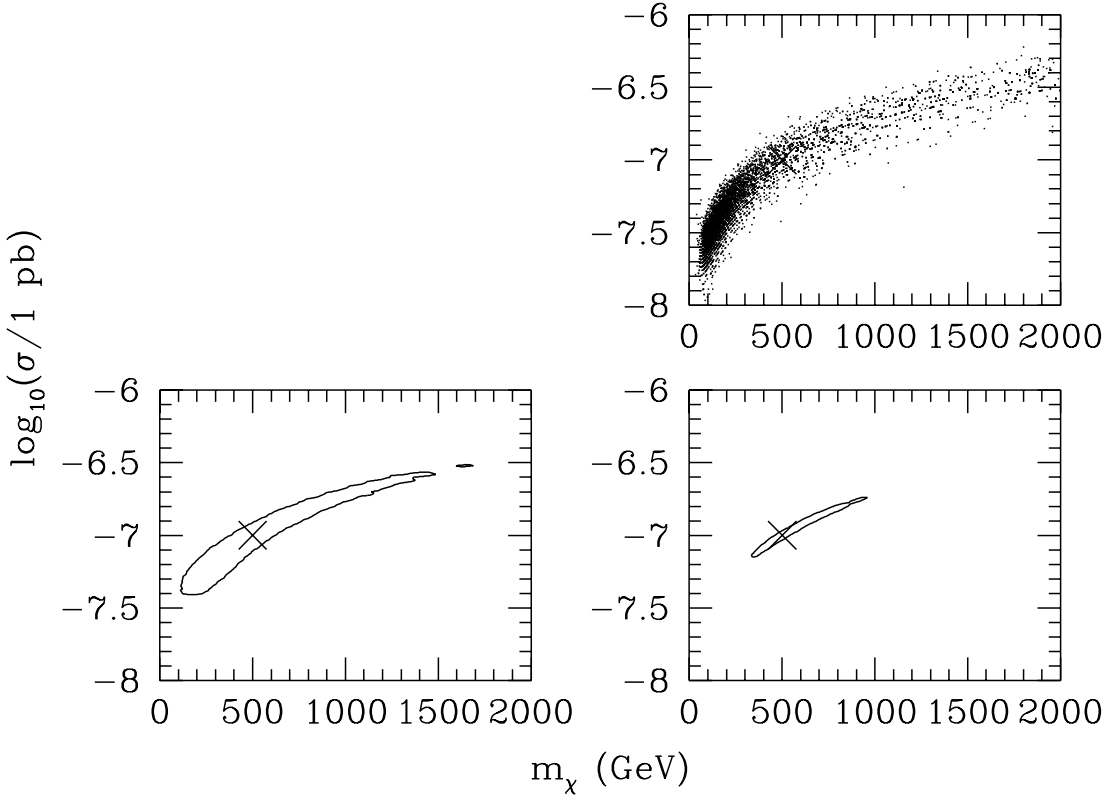


Figure 6. As fig. 2 for $m_\chi = 500$ GeV. For $\mathcal{E} = 3 \times 10^2$ kg day, $\lambda_{\text{in}} = 2.4$. Consequently $\sim 10\%$ experiments would not detect any events and even for the other experiments the number of events is typically too small to obtain meaningful constraints on the WIMP parameters (hence there is no plot for this exposure). Even for $\mathcal{E} = 3 \times 10^5$ kg day there is a large tail of experiments with large m_χ values and hence it is not possible to plot a contour containing 95% of events.

In fig. 7 we show the effect of the uncertainty in the value of the local circular speed, v_c , on the determination of m_χ . For an input WIMP mass of $m_\chi = 100$ GeV and an exposure of $\mathcal{E} = 3 \times 10^3$ kg day we vary v_c between 180 and 260 km s^{-1} [22]. The likelihood analysis is however carried out assuming $v_c = 220$ km s^{-1} . For larger (smaller) v_c the incoming WIMPs have larger (smaller) typical kinetic energies than assumed, resulting in larger (smaller) best fit mass values. More qualitatively, differentiating the expression for E_r , eq. (8),:

$$\frac{\Delta v_c}{v_c} = -\frac{\Delta m_\chi}{m_\chi [1 + (m_\chi/m_A)]}, \quad (10)$$

which gives, for an input WIMP mass of $m_\chi = 100$ GeV a ~ 20 GeV shift in the WIMP mass from a 20 km s^{-1} uncertainty in v_c . However, as we see in fig. 7, the shape of the distribution of the best fit parameters changes, in qualitatively the same way as when the underlying WIMP mass is changed. As v_c is decreased (increased) the expected

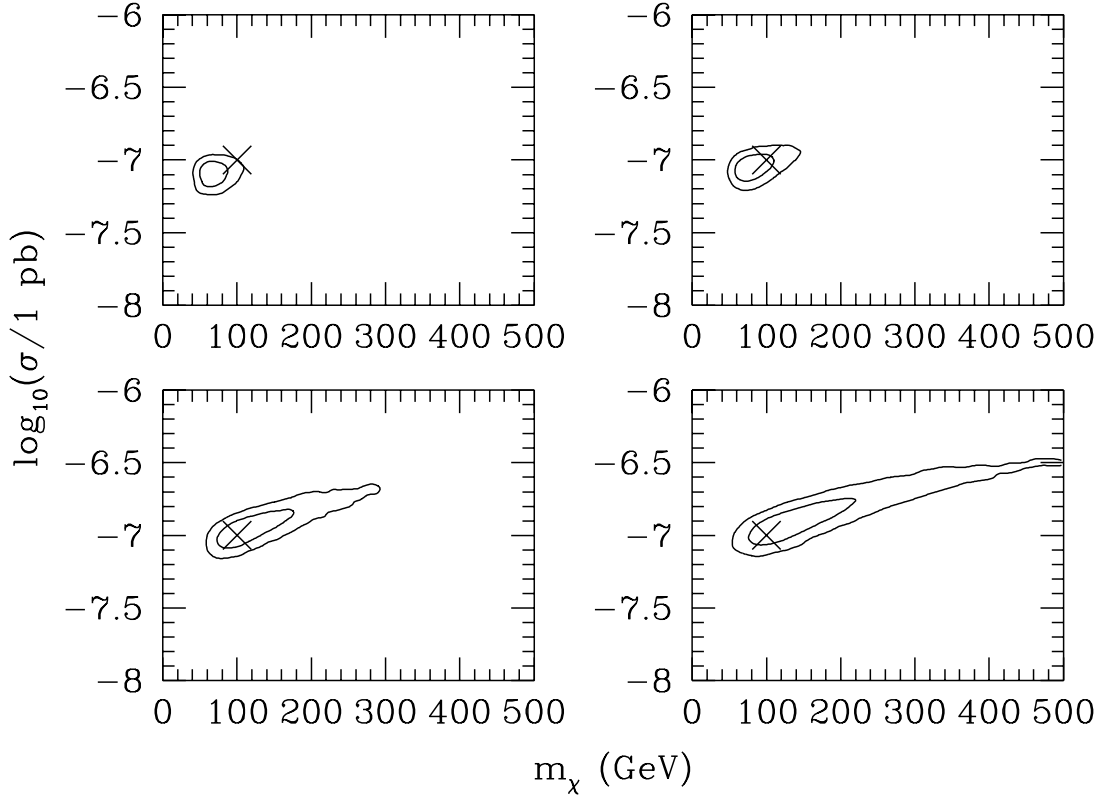


Figure 7. As fig. 2 but varying the input circular velocity $v_c = 180, 200, 240$ and 260 km s^{-1} with the exposure fixed at $\mathcal{E} = 3 \times 10^3 \text{ kg day}$. The maximum likelihood analysis is carried out assuming $v_c = 220 \text{ km s}^{-1}$.

number of events increases (decreases) and hence the best-fit cross-sections typically decrease (increase).

Finally in fig. 8 we examine the effect of the uncertainty in the detailed shape of the local velocity distribution. For an input WIMP mass of $m_\chi = 100 \text{ GeV}$ and the largest exposure, $\mathcal{E} = 5 \times 10^5 \text{ kg day}$, we use as input the logarithmic ellipsoidal model (which is the simplest triaxial generalization of the standard isothermal sphere) [25] and two of the sets of parameter values previously considered in Ref. [26]: $p = 0.9, q = 0.8, \gamma = 0.07$ and $p = 0.72, q = 0.7, \gamma = 4.0$ with the Earth located on the intermediate axis. These parameters correspond to axial ratios $1 : 0.78 : 0.48$ and $1 : 0.45 : 0.38$ (i.e. quite extreme triaxiality, especially in the second case) and, in both cases, velocity anisotropy $\beta = 0.1$. The local circular and escape speeds are kept fixed at the values used for the standard halo model. The likelihood analysis is carried out assuming the standard Maxwellian velocity distribution. Even for the second, quite extreme, model the shift in the typical best fit mass from the underlying value is relatively small (less than 5 GeV). The small increase in the expected number of events for these halo models leads to a small downwards shift in the distribution of best-fit cross-sections.

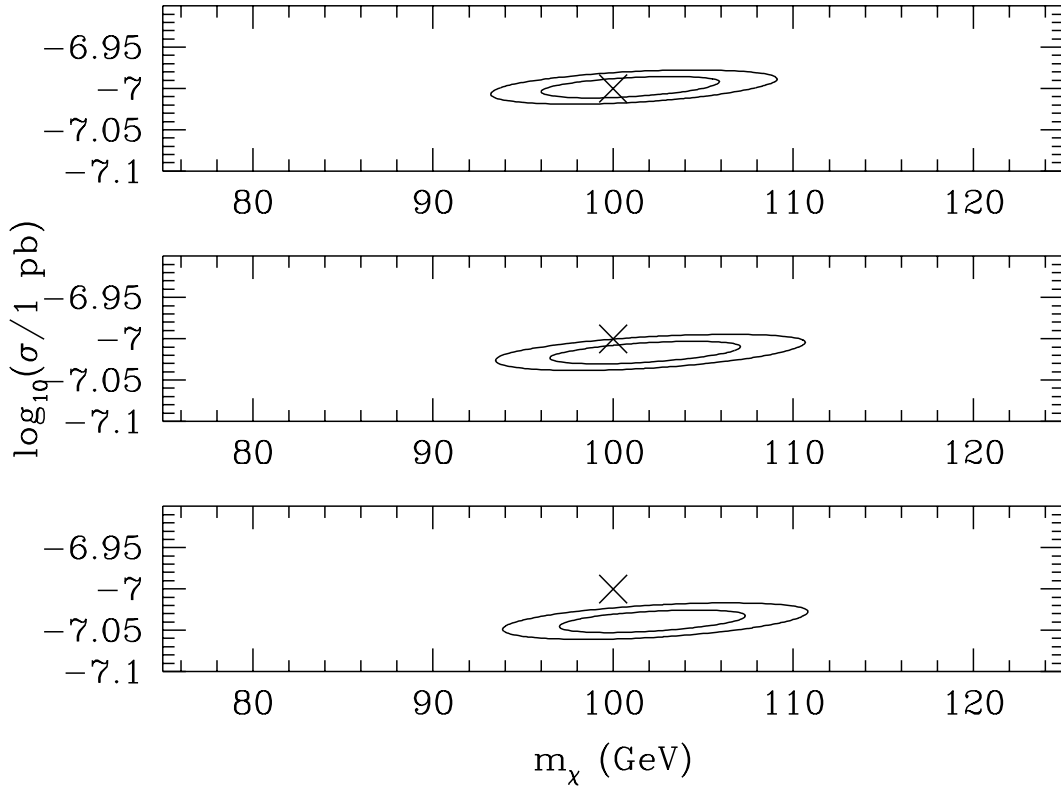


Figure 8. As fig. 7 but for the standard halo model (top panel) and the two non-standard halo models described in the text with the exposure fixed at $\mathcal{E} = 3 \times 10^5$ kg day. The maximum likelihood analysis is carried out assuming the standard Maxwellian speed distribution.

4. Validity of assumptions

4.1. WIMP distribution

Since the differential event rate is directly proportional to $\rho_\chi \sigma_p$, any uncertainty in the local WIMP density leads straightforwardly to an equivalent uncertainty in σ_p . We have fixed the local WIMP density to the ‘standard value’ of $\rho_\chi = 0.3$ GeV cm $^{-3}$. Refs. [27, 28] found, using various observations to constrain the parameters of a range of halo models, local densities in the range 0.2 – 0.8 GeV cm $^{-3}$, which would lead to a factor of a few uncertainty in the determination of the cross-section.

We saw above that an uncertainty in the local circular velocity translates directly into an uncertainty in the measured WIMP mass. The smooth halo models typically considered in the literature have *time averaged* differential event rates which are very similar to that found under the standard assumption of a Maxwellian velocity distribution (e.g. [29, 26]). Hence, as we saw above, the uncertainty in the speed distribution, for fixed v_c , only leads to a small systematic error in the determination

of the WIMP mass (see fig. 8). These smooth halo models are derived by solving the collisionless Boltzmann equation which assumes that the dark matter distribution has reached a steady state. The assumption that the local dark matter distribution is dynamically mixed, and hence smooth, is, however, a strong assumption, which may not be valid [30, 31]. Direct detection experiments probe the dark matter distribution on sub-milli-pc scales. Numerical simulations, however, have only of order 100 ‘particles’ per kpc^{-3} (see e.g. Ref. [32]) in the solar neighbourhood and hence can not resolve the dark matter distribution on the relevant scales.

In CDM cosmologies structure forms hierarchically and the local dark matter distribution will depend on the fate of the first, smallest, WIMP micro-halos to form. The mass of these microhalos is set by the WIMP microphysics in the early Universe [33], specifically kinetic decoupling and free-streaming, and (depending on the WIMP’s interaction properties) is expected to lie in the range $10^{-12}M_\odot$ to $10^{-4}M_\odot$ [34]. The dynamical evolution of these micro-halos is being studied [35], however the detailed dark matter phase space distribution on sub-milli-pc scales is not yet known with any degree of certainty. If the local dark matter distribution consists of a small number of streams, with a-priori unknown velocities, then the energy spectrum would consist of a series of (sloping due to the energy dependence of the form factor) steps and extracting information on the WIMP mass and cross-section from experimental data would be difficult.

4.2. Zero background

From an experimental point of view, the most significant assumption is probably that of zero background. Non-zero background could be incorporated (c.f. Ref. [36]) by simulating the recoil spectra produced by neutrons and including the background event rate (and possibly additional parameters modeling the spectrum of the background events) in the maximum likelihood analysis. This would, however, require detailed modeling of the detector set-up and shielding.

4.3. Other sources of systematic error

Finite energy resolution and uncertainty in the form factor are other potential experimental sources of systematic error. The Helm form factor, with parameter values as advocated by Lewin and Smith [7], deviates by only of order 1% from that calculated using electron elastic scattering data [37]. We have checked that Gaussian energy resolution, with full width at half maximum of order 1 keV [14], does not systematically affect the WIMP parameters extracted from the energy spectrum. Both of these issues are therefore likely to be less important than non-zero background and/or fine-grained structure in the WIMP distribution.

From a theoretical point of view the WIMP may have spin-dependent interactions ¶

¶ Natural Germanium contains 7.7% ^{73}Ge which is sensitive to spin dependent interactions [39].

with the nucleon and/or different coupling to the proton and neutron (e.g. Ref. [38, 39]). The measurement of the WIMP mass, in principle, in this case has been considered in Ref. [20].

5. Summary

We have examined the accuracy with which it will be possible to determine the WIMP mass from the energy spectrum observed in a SuperCDMS-like direct detection experiment. The differential event rate varies with energy, modulo the energy dependence of the detector form factor, as $dR/dE \propto \exp(-E/E_R)$ where the characteristic energy, E_R , depends on the WIMP mass, m_χ . For light WIMPs, $m_\chi \ll m_A$ where m_A is the mass of the target nuclei, $E_R \propto m_\chi^2$, while for heavy WIMPs, $m_\chi \gg m_A$, $E_R \sim \text{const}$. Consequently for light WIMPs the energy spectrum is strongly dependent on the WIMP mass, allowing the mass to be measured fairly accurately. For heavy WIMPs the dependence on the WIMP mass is far weaker making it difficult to measure the mass.

We have carried out Monte Carlo simulations of a SuperCDMS-like experiment composed of a Ge target with an energy threshold of 10 keV and zero background. We assumed, initially, that the local WIMP density is known and that the WIMP speed distribution is Maxwellian with local circular velocity $v_c = 220 \text{ km s}^{-1}$. For an optimistic interaction cross-section of $\sigma_p = 10^{-7} \text{ pb}$, just below the current exclusion limits from the CDMS experiment [12], we considered a range of WIMP masses, $25 \text{ GeV} < m_\chi < 500 \text{ GeV}$, and, efficiency weighted, exposures, $3 \times 10^2 \text{ kg day} < \mathcal{E} < 3 \times 10^5 \text{ kg day}$. For $\mathcal{E} = 3 \times 10^2 \text{ kg day}$ the expected number of events is small, the best fit masses and cross-sections are stratified on parabolas of constant number of events and it would not be possible to obtain better than order of magnitude constraints on the WIMP parameters. For $\mathcal{E} = 3 \times 10^5 \text{ kg day}$ and an input mass of $m_\chi = 100 \text{ GeV}$ it would be possible, given the validity of the assumptions stated above, to measure the WIMP mass with accuracy $\pm 10 \text{ GeV}$ and the fractional cross-section with accuracy $\Delta(\log \sigma_p) = \pm 0.02$. The mass of lighter WIMPs could be measured more accurately, however for very light WIMPs, $m_\chi < \mathcal{O}(10 \text{ GeV})$, the number of events above the detector energy threshold would be too small to allow the mass to be measured accurately. For more massive WIMPs there is a significant tail of experiments with best fit masses significantly larger than the input WIMP mass. For heavy WIMPs, $m_\chi > \mathcal{O}(500 \text{ GeV})$, even with $\mathcal{E} = 3 \times 10^5 \text{ kg day}$ it will only be possible to place lower limits on the WIMP mass and cross-section.

We then examined the effect of varying the underlying WIMP speed distribution for an input WIMP mass of 100 GeV. A change of $\pm 20 \text{ km s}^{-1}$ in the local circular speed, v_c , leads to a shift in the distribution of best fit WIMP mass of roughly $\pm 20 \text{ GeV}$ (although an increase in v_c leads, like an increase in the underlying WIMP mass, to a large tail of experiments with large best fit masses). Changing the shape of the WIMP velocity distribution, while keeping v_c fixed, leads to only a small change in the input energy spectrum and hence the shift in the best fit WIMP masses is relatively small,

$< \mathcal{O}(5 \text{ GeV})$, even for quite extreme smooth halo models. There is, for smooth halo models, a factor of a few uncertainty in the local WIMP density [27, 28] which leads to a corresponding uncertainty in σ_p . The assumption of a smooth WIMP distribution may well, however, not be valid. The local WIMP distribution, on sub milli-pc scales, may be composed of a (a priori unknown) number of discrete streams with unknown velocities. If this is the case it will be difficult to extract constraints on the WIMP mass from an observed signal.

Finally we discussed the validity of the other assumptions made, namely zero background, purely spin independent coupling, perfect energy resolution and known detector form factor. Of these zero background is probably the most significant and could in principle be taken into account by simulating the recoil spectra produced by neutrons and including the background event rate (and possibly background spectrum shape) in the maximum likelihood analysis.

Acknowledgments

AMG is supported by PPARC and is grateful to Ben Morgan and Simon Goodwin for useful discussions and Meghan Gray and Chris Conselice for assistance with supermongo contour plotting.

6. References

- [1] M. Tegmark et al., Phys. Rev. D **69** 103501 (2004), [astro-ph/0310723](#); D. J. Eisenstein et al., Astrophys. J **633**, 560 (2005), [astro-ph/0501171](#); S. Cole et al., Mon. Not. Roy. Astron. Soc. **362**, 505 (2005), [astro-ph/0501174](#); D. N. Spergel et al., [astro-ph/0603449](#).
- [2] G. Jungman, M. Kamionkowski and K. Griest, Phys. Rep. **267**, 195 (1996).
- [3] L. Bergström, Rept. Prog. Phys. **63**, 793 (2000), [hep-ph/0002126](#); G. Bertone, D. Hooper and J. Silk, Phys. Rep. **405** 279 (2005), [hep-ph/0404175](#).
- [4] M. W. Goodman and E. Witten, Phys. Rev. D **31**, 3059 (1985).
- [5] E. A. Baltz, M. Battaglia, M. E. Peskin and T. Wizansky, Phys. Rev. D **74** 103521 (2006), [hep-ph/0602187](#).
- [6] D. Hooper and A. M. Taylor, [hep-ph/0607086](#); M. Carena, D. Hooper and A. Vallinoto, [hep-ph/0611065](#).
- [7] J. D. Lewin and P. F. Smith, Astropart. Phys. **6**, 87 (1996).
- [8] A. K. Drukier, K. Freese and D. N. Spergel, Phys. Rev. D **33**, 3495 (1986); K. Freese, J. Frieman and A. Gould, Phys. Rev. D **37**, 3388 (1988).
- [9] J. R. Primack, D. Seckel and B. Sadoulet, Ann. Rev. Nucl. Part. Sci. **38**, 751 (1988).
- [10] F. Hasenbalg, Astropart. Phys. **9**, 339 (1998), [astro-ph/9806198](#).
- [11] M. J. Lewis and K. Freese, Phys. Rev. D **70** 043501 (2004), [astro-ph/0307190](#).
- [12] D. S. Akerib et al., Phys. Rev. Lett. **96** 011302 (2006), [astro-ph/0509269](#).
- [13] D. S. Akerib et al., Phys. Rev. D **72**, 052009 (2005), [astro-ph/0507190](#).
- [14] R. W. Schnee et al., proceedings of DARK 2004, fifth international Heidelberg conference on dark matter in Astro and Particle Physics, [astro-ph/0502435](#).
- [15] P. L. Brink et al., proceedings of Texas Symposium on Relativistic Astrophysics (2004), [astro-ph/0503583](#).
- [16] E. Aprile et al., [astro-ph/0502279](#).
- [17] H. Kraus et al., J. Phys. Conf. Ser. **39** 139 (2006).

- [18] Y. Ramachers, *Astroparticle Physics* **19**, 419 (2003).
- [19] R. Bernabei et al., *Phys. Lett.* **B389**, 757 (1996); *ibid* **B408**, 439 (1997); *ibid* **B424**, 195 (1998); *ibid* **B450**, 448 (1999); *ibid* **B480**, 23 (2000). R. Bernabei et al., *Riv. Nuovo. Cim.* **26N1** 1 (2003), [astro-ph/0307403](#).
- [20] J. L. Bourjaily and G. L. Kane, [hep-ph/0501262](#).
- [21] R. H. Helm, *Phys. Rev.* **104** 1466 (1956).
- [22] F. J. Kerr and D. Lynden-Bell, *Mon. Not. Roy. Astron. Soc.* **221**, 1023 (1986).
- [23] M. C. Smith et al., [astro-ph/0611671](#).
- [24] G. Cowan, *Statistical data analysis*, published by Oxford University Press (1998).
- [25] N. W. Evans, C. M. Carollo and P. T. de Zeeuw, *Mon. Not. Roy. Astron. Soc.* **318**, 1131 (2000), [astro-ph/0008156](#).
- [26] A. M. Green, *Phys. Rev. D* **66**, 083003 (2002), [astro-ph/0207366](#).
- [27] E. I. Gates, G. Gyuk and M. S. Turner, *Astrophys. J.* **449**, L123 (1995), [astro-ph/9505039](#).
- [28] L. Berström, P. Ullio and J. H. Buckley, *Astropart. Phys.* **9** 137 (1998), [astro-ph/9712318](#).
- [29] M. Kamionkowski and A. Kinkhabwala, *Phys. Rev. D* **57**, 3256 (1998), [hep-ph/9710337](#).
- [30] B. Moore et al., *Phys. Rev. D* **64** 063508 (2001), [astro-ph/0106271](#).
- [31] S. Stiff and L. Widrow, *Phys. Rev. Lett.* **90**, 211301 (2003), [astro-ph/0301301](#).
- [32] A. Helmi, S. D. M. White and V. Springel, *Phys. Rev. D* **66**, 0635023 (2002), [astro-ph/0201289](#).
- [33] S. Hofmann, D. Schwarz and H. Stöcker, *Phys. Rev. D* **64** 083507 (2001), [astro-ph/0104173](#); V. Berezinsky, V. Dokuchaev and Y. Eroshenko, *Phys. Rev. D* **68** 103003 (2003), [astro-ph/0301551](#); A. M. Green, S. Hofmann and D. J. Schwarz, *Mon. Not. Roy. Astron. Soc.* **353**, L23 (2004), [astro-ph/0309621](#); *JCAP* 0508 (2005) 003, [astro-ph/0508553](#); A. Loeb and M. Zaldarriaga, *Phys. Rev. D* **71** 103520 (2005), [astro-ph/0504112](#); E. Bertschinger, *Phys. Rev. D* **74** 063509 (2006), [astro-ph/0607319](#).
- [34] S. Profumo, K. Sigurdson and M. Kamionkowski, *Phys. Rev. Lett.* **97** 031301 (2006), [astro-ph/0603373](#).
- [35] J. Diemand, B. Moore and J. Stadel, *Nature* **433**, 389 (2005), [astro-ph/0501589](#); V. Berezinsky, V. Dokuchaev and Y. Eroshenko, *Phys. Rev. D* **73** 063504 (2006), [astro-ph/0511494](#); H. Zhao, D. Hooper, G. W. Angus, J. E. Taylor and J. Silk, *Astrophys. J.* **654**, 697 (2007), [astro-ph/0508215](#); A. M. Green and S. P. Goodwin, *Mon. Not. Roy. Astron. Soc.* **376**, 1111 (2007), [astro-ph/0604142](#); T. Goerdt, O. Y. Gnedin, M. Moore, J. Diemand and J. Stadel, *Mon. Not. Roy. Astron. Soc.* **375**, 191 (2007), [astro-ph/0608495](#); G. W. Angus and H. Zhao, *Mon. Not. Roy. Astron. Soc.* **375**, 1146 (2007), [astro-ph/0608580](#).
- [36] H. Kraus et al., *Phys. Lett. B* **610** 37 (2005).
- [37] G. Duda, A. Kemper and P. Gondolo, [hep-ph/0608035](#).
- [38] P. Ullio, M. Kamionkowski and P. Vogel, *J. High Energy Phys.* **07**:044 (2001), [hep-ph/0010036](#); A. Kurylov and M. Kamionkowski, *Phys. Rev. D* **69**, 063503 (2004), [hep-ph/0307185](#); F. Giuliana, *Phys. Rev. Lett.* **93**, 161301 (2004), [hep-ph/0405215](#); C. Savage, P. Gondolo and K. Freese, *Phys. Rev. D* **70**, 123513 (2004), [astro-ph/0408346](#).
- [39] D. S. Akerib et al., *Phys. Rev. D* **73**, 011102 (2006), [astro-ph/0509269](#).